Observability Analysis of Data Reconstruction Strategies for a Cardiac Ionic Model

Laura M Muñoz[1], Anna E Marks[2], Julio A Santiago-Reyes[3], Mark O Ampofo[1], Elizabeth M Cherry[4,1]

[1]Rochester Institute of Technology, Rochester, NY, USA
[2]Wake Forest University, Winston-Salem, NC, USA
[3]The College of New Jersey, Ewing, NJ, USA
[4]Georgia Institute of Technology, Atlanta, GA, USA

Abstract

The study of arrhythmia formation is impeded by limitations in sensor technology, since not all quantities of interest can be measured directly from the same cell or tissue preparation. Data assimilation algorithms can reconstruct unmeasured quantities by combining model predictions with available data. However, it is not clear which types of measurements are best for reconstructing data, or how abnormal action-potential patterns, such as alternans, affect the informativeness of measurements. To address these issues, we examined the Shiferaw-Sato-Karma (SSK) cardiac myocyte model, which can be used to simulate multiple alternans mechanisms. We conducted a numerical study in which each SSK dynamical variable was considered to be a source of simulated data, and computed observability measures, where observability is a control-theoretic model property that indicates whether unmeasured quantities can be reconstructed from a measured variable. Although the best measurements (in the sense of maximizing observability) varied depending on alternans mechanism (voltage- or calcium-driven), we found that some patterns held for both mechanisms, such as intracellular calcium concentration yielding stronger observability than membrane potential. Observability strengths also typically predicted the relative performances of Kalman-filter-based assimilators for different measurement types.

1. Introduction

Electrical alternans, which is a beat-to-beat alternation in cardiac action potential (AP) duration, sometimes precedes dangerous arrhythmias such as ventricular fibrillation. Alternans may arise from different mechanisms, including instabilities in the dynamics of the cellular membrane potential (referred to here as voltage-driven alternans) or intracellular calcium ionic concentrations (calcium-driven alternans). In electrophysiological experiments, it is not generally possible to record all quantities that may contribute to alternans or arrhythmia formation. Data assimilation algorithms, which combine forecasts from dynamical models with corrective adjustments based on available measurements, can be used to reconstruct quantities that are not recorded during an experiment. Data assimilators have been designed for a variety of cardiac inference problems, including the reconstruction of transmural excitation patterns based on optical mapping data [1].

A related question is which sensor locations and types of data will maximize the accuracy of estimates produced by an assimilation algorithm. To help answer this question, we analyzed the observability of a cardiac myocyte model. Observability is a control-theoretic model property that quantifies how well the state of a dynamical system can be reconstructed from a set of measurements. Before designing an assimilation algorithm, it is helpful to choose measurements that maximize observability of the predictive model that is embedded in the assimilation algorithm, in order to improve the quality of estimated quantities.

Observability studies of cardiac action-potential models (e.g., [2]) are relatively rare, and to our knowledge, only our group has examined observability of a myocyte model that has detailed intracellular calcium handling [3]. Our previous work did not account for the possible impact of different alternans mechanisms on observability, so in the present work, we analyzed the Shiferaw-Sato-Karma (SSK) model [4], which can represent multiple alternans mechanisms. The main original contributions of this paper are an evaluation of the effects of voltage- and calcium-driven alternans mechanisms on the observability properties of a cardiac ionic model, along with an assessment of how well our observability measures predicted the performance of a Kalman-filter-based data assimilation algorithm under different alternans conditions. The present

work is a companion paper to our earlier study [5], where we computed a different kind of control-theoretic property (called controllability) of the SSK model to determine best strategies for suppressing alternans.

2. Methods

The Shiferaw-Sato-Karma (SSK) myocyte model [4] is a system of nonlinear ordinary differential equations that may be written as $\dot{X} = f(X, I_{stim}(t))$. The state vector, which contains the model's sixteen state variables, is $X = [V\ m\ h\ j_{Na}\ X_r\ X_s\ X_{to}\ Y_{to}\ d\ f\ q\ c_s\ c_{int}\ c_{sr}\ c'_{jsr}\ I_{rel}]^T$. The state variables are the membrane potential V (mV), dimensionless gating variables m, h, j_{Na}, X_r, X_s, X_{to}, Y_{to}, d, f, and q, Ca^{2+} concentrations (μM) in the submembrane space (c_s), bulk myoplasm (c_{int}), and sarcoplasmic reticulum (SR) including network and junctional SR (NSR and JSR) volumes (c_{sr}), average JSR calcium concentration of compartments not being drained (c'_{jsr}), and total SR release current I_{rel} ($\mu M/s$). The independent variable is time, t (ms). To induce APs, we applied stimulus current $I_{stim}(t)$ (mV/ms), which was a period-T rectangular pulse train (settings are described further by Cherry [6]). Two configurations of model parameters were adopted from another source [7] to yield alternans that was either voltage-driven or calcium-driven. Examples are shown in Figure 1. All computations were performed in MATLAB.

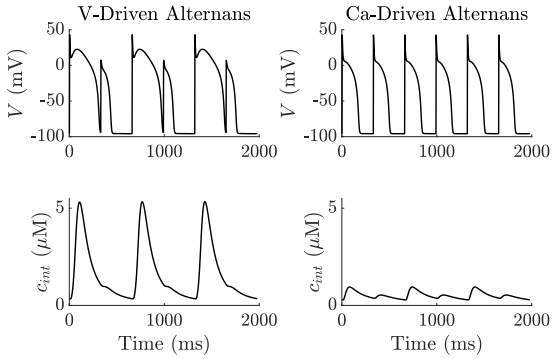

Figure 1: SSK model output from pacedown protocol described by Cherry [6]. Left: voltage-driven alternans, right: calcium-driven alternans. Top: V vs. t, bottom: c_{int} vs. t after pacing at $T = 330$ ms for 2 min (actual times are those shown in graph plus a 2-min offset).

To assist with computations, a discrete-map form of the SSK model, $X((j+1)T) = F(X(jT))$, was produced by numerically time-integrating the ODEs over one period, T, using explicit Euler and Rush-Larsen schemes with integration time step 0.01 ms, where $j = 0, 1, 2, ...$ is the period index. Fixed points (solutions to $X^* = F(X^*)$) were estimated and the model was numerically linearized about X^* using methods described in our previous work [3]. The resulting linearized dynamical equation was $x_{j+1} = Ax_j + B_\nu \nu_j$ with output equation $y_j = Cx_j + \varepsilon_j$. Here, we defined the deviational state vector as $x_j = X_j - X^*$, with state matrix $A = \partial F/\partial X|_{X^*}$. The output matrix, C, encodes the choice of measured variable, and y represents the simulated measurement. ν_j and ε_j are white, zero-mean, independent, and normally distributed process and sensor noise signals with variances Q and R, and $B_\nu = I$ is the process noise input matrix. The linearized equations were nondimensionalized using a procedure described elsewhere [3], and subsequent references to x, A, C, etc., refer to quantities in the nondimensional equations.

A system is said to be observable from y if we can always uniquely determine initial state x_0 from a sufficiently long but finite time-series of measurements, $y_1, y_2, ..., y_n$. We computed a modal observability measure [8], $|\cos\phi_{i,k}| = |C_i \cdot v_k|/(\|C_i\|\|v_k\|)$, which (if nonzero) means the k-th eigenvalue (referred to here as a "mode") is observable from the i-th measured variable, where λ_k and v_k are the k-th eigenvalue and right eigenvector of A. We considered each state variable as a hypothetical source of measurements, leading to a total of 16 different measurement types, where each type was represented by selecting C_i as the i-th row of the identity matrix. For example, $C_i = C_1 = [1\ 0\ ...\ 0]$ means that the first state variable, V, is measured every T ms. Larger $|\cos\phi_{i,k}|$ values in the $[0, 1]$ range mean that the contribution of the k-th mode to the system response is more strongly observable from the i-th variable. Different measurement types were ranked according to their average observability values, $|\cos\phi_i|$, defined here as the mean of all $|\cos\phi_{i,k}|$ values for which $|\lambda_k| > 0.9$. We only included larger modes in the averages, since those modes contribute more substantively to the evolution of x_j from one period to the next.

We examined the Kalman filter (KF) and related methods for reconstructing simulated data. Specifically, we tested a linear estimator that produces state estimates $\hat{x}$ via $\hat{x}_{j+1} = A\hat{x}_j + L(y_j - C\hat{x}_j)$, where L is the gain matrix. For each type of measurement, we computed a preliminary KF gain, L_{KF}, by applying MATLAB'S `kalman` function to the nondimensional system and noise-covariance matrices, assuming $Q = 0.1I$ and $R = 0.01$. To allow for fairer comparisons across measurement types, we followed a procedure similar to that of [3] to replace KF gain L_{KF} with a modified gain L using MATLAB's `place` function. For each measurement type, L was chosen to ensure that the closed-loop eigenvalues, which were the eigenvalues of $A - LC_i$, had a maximum modulus of 0.7.

For each measurement type, we compared observability values to two estimator performance measures: feedback effort, $\|LC\|$, and $\langle\|e\|\rangle$, an average norm of simulated es-

timation error $e_j = x_j - \hat{x}_j$. $\|e_j\|$ was calculated for the last cycle of a 30-period simulation, with noise signals set to zero to facilitate comparisons. Final $\|e\|$ values were averaged over 10 simulations with randomly-chosen initial conditions, yielding an average norm $\langle\|e\|\rangle$. Smaller values are preferred for each performance measure.

3. Results and Discussion

The different choices of measured variable are ranked in decreasing order of observability strength in Table 1. The values were calculated for $T = 330$ ms, which is a stimulus period that yields long-range alternans for both the voltage- and calcium-driven parameter sets, as suggested by Figure 1 and in bifurcation plots shown elsewhere [6]. Table 1 shows that measuring the slow sodium inactivation gate (j_{Na}) maximized observability of the larger modes for voltage-driven alternans, while measuring the submembrane calcium concentration (c_s) yielded strongest observability for the calcium-driven case. Many of the variables, including gating variables such as j_{Na}, are not directly measurable, but are included here for completeness. Despite the alternans mechanism affecting the observability rankings, certain patterns were evident across mechanisms. For example, when comparing two lab-accessible quantities, V and c_{int}, Table 1 shows that c_{int} yielded stronger observability than V for either mechanism. This ordering of the two variables appears to be consistent with our previous observability analysis [3] of a different myocyte model, the Luo-Rudy dynamic (LRd) model (2009 version) [9].

Two performance measures, feedback effort and average final error, are plotted against observability values in Figure 2. The plots show that a larger observability value typically predicted better performance (in the sense of smaller $\|LC\|$ and $\langle\|e\|\rangle$ values). This result demonstrates that observability values can often be used to predict which type of measurement will yield the best data assimilation algorithm performance, which is helpful because computing observability measures only requires knowledge of model matrices A and C, whereas the KF-based assimilator design requires estimates of noise covariance matrices and additional computational steps to produce gain matrices L. These relationships among observability and linear assimilator performance measures are already well-known within the control systems community, but were examined here since they have only rarely been explored for cardiac electrophysiological models.

In the calcium-driven alternans plot in Figure 2, the measurement choice of d was omitted since it was the only combination of measurement type and parameter set for which we were unable to design a KF gain (the `kalman` function returned an error). Measuring d for calcium-driven alternans yielded the smallest value (-7.83) in Table 1, so presumably the observability was too weak to allow for gain computation.

Voltage Driven Alternans		Calcium Driven Alternans	
Meas. var. (i)	lg $\lvert\cos\phi_i\rvert$	Meas. var. (i)	lg $\lvert\cos\phi_i\rvert$
j_{Na}	-0.010571	c_s	-0.116682
c_s	-0.917632	c'_{jsr}	-0.352230
f	-1.038123	c_{sr}	-0.406352
c'_{jsr}	-1.065499	c_{int}	-0.912790
c_{sr}	-1.103919	j_{Na}	-1.414577
c_{int}	-1.149056	q	-1.803661
X_r	-1.749180	X_r	-2.048024
X_s	-1.785763	X_s	-3.073488
q	-1.854422	V	-3.286332
Y_{to}	-2.266038	f	-4.103333
V	-2.853644	h	-4.691668
I_{rel}	-3.698748	I_{rel}	-5.132808
h	-4.201480	m	-5.418449
m	-5.025919	X_{to}	-6.576203
X_{to}	-6.123031	Y_{to}	-7.437371
d	-6.705204	d	-7.831259

Table 1: Measured variables ranked in decreasing strength of modal observability, lg$|\cos\phi_i|$, where lg is base-10 logarithm. Results shown for $T = 330$ ms and averaged over all modes for which $|\lambda_k| > 0.9$.

One limitation of our work is that stronger observability did not always predict smaller performance measures; for example, in the calcium-driven alternans plot in Figure 2, X_r yielded worse observability than q, yet the X_r-based estimator outperformed the q-based estimator. This lack of correspondence is likely due to our choice of observability measure, which includes ad-hoc averaging over larger modes. When a gain L is designed to reassign only one eigenvalue λ_k of A, we expect quantities such as feedback effort to decrease as $|\cos\phi_{i,k}|$ increases, but this kind of relationship is not assured when multiple eigenvalues are reassigned and modal observability values are averaged, as in our tests. Relationships between observability and performance measures for single and multiple-eigenvalue reassignment scenarios were explored in more detail in our study of the LRd model [3]. Figure 2 shows that our chosen observability measure is capable of predicting which measurements will yield better estimator performance in cases where the observability values are well-separated. In future work, we could investigate whether other methods for aggregating observability values lead to improved predictions of assimilator performance.

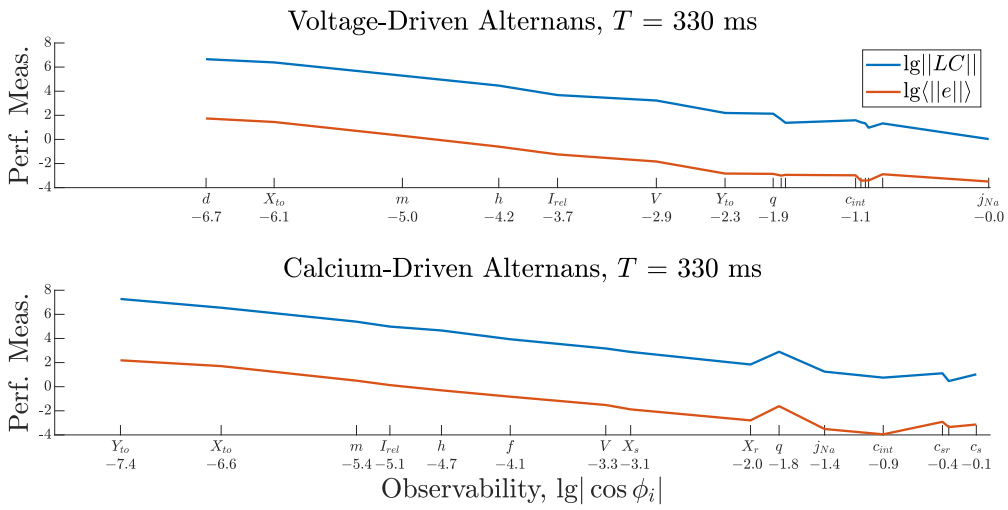

Figure 2: Performance measures lg$\|LC\|$ and lg$\langle\|e\|\rangle$ vs. observability measure lg$|\cos\phi_i|$, for each measurement type for which we were able to compute L. Top: Voltage-driven alternans, bottom: calcium-driven alternans. Certain axis labels were suppressed to improve readability.

4. Conclusions

We found that alternans mechanisms (voltage vs. calcium-driven) affected observability-based rankings of best measurement strategies for the Shiferaw-Sato-Karma myocyte model. When comparing certain lab-accessible measurements (c_{int} and V) we found that c_{int} was a more informative measurement type, in the sense of yielding stronger observability, for both types of alternans. Stronger observability typically corresponded with better data assimilator performance, which is a helpful result because it shows that observability analysis can help researchers to determine which data types will be more informative, before steps are taken to design a data assimilation algorithm.

Acknowledgments

This work was supported, in part, by the National Science Foundation under Grant Nos. 2243938, CNS-1446312, and CNS-2028677.

References

[1] Marcotte CD, Hoffman MJ, Fenton FH, Cherry EM. Reconstructing cardiac electrical excitations from optical mapping recordings. Chaos An Interdisciplinary Journal of Nonlinear Science September 2023;33(9):093141. ISSN 1054-1500, 1089-7682.

[2] Marcotte CD, Grigoriev RO. Adjoint eigenfunctions of temporally recurrent single-spiral solutions in a simple model of atrial fibrillation. Chaos An Interdisciplinary Journal of Nonlinear Science September 2016;26(9):093107. ISSN 1054-1500, 1089-7682.

[3] Guzman A, Vogt R, Charron C, Pusarla K, Muñoz L. Observability analysis and state observer design for a cardiac ionic cell model. Computers in Biology and Medicine October 2020;125:103910. ISSN 00104825.

[4] Shiferaw Y, Sato D, Karma A. Coupled dynamics of voltage and calcium in paced cardiac cells. Physical Review E February 2005;71(2):021903. ISSN 1539-3755, 1550-2376.

[5] Muñoz LM, Ampofo MO, Cherry EM. Controllability of voltage- and calcium-driven alternans in a cardiac ionic model. In Computing in Cardiology, volume 49. 2022; 1–4.

[6] Cherry EM. Distinguishing mechanisms for alternans in cardiac cells using constant-diastolic-interval pacing. Chaos An Interdisciplinary Journal of Nonlinear Science September 2017;27(9):093902. ISSN 1054-1500, 1089-7682.

[7] Groenendaal W, Ortega FA, Krogh-Madsen T, Christini DJ. Voltage and calcium dynamics both underlie cellular alternans in cardiac myocytes. Biophysical Journal May 2014; 106(10):2222–2232. ISSN 00063495.

[8] Hamdan AMA, Nayfeh AH. Measures of modal controllability and observability for first- and second-order linear systems. Journal of Guidance Control and Dynamics 1989; 12(3):421–428.

[9] Livshitz L, Rudy Y. Uniqueness and stability of action potential models during rest, pacing, and conduction using problem-solving environment. Biophysical Journal 2009; 97(5):1265–1276. ISSN 0006-3495.

Address for correspondence:

Laura Muñoz
Rochester Institute of Technology
85 Lomb Memorial Drive, Rochester, NY, USA, 14623
laura.m.munoz@gmail.com